Food Research International 157 (2022) 111267

Contents lists available at ScienceDirect

Food Research International

journal homepage: www.elsevier.com/locate/foodres

Structural characterization and anti-photoaging activity of a polysaccharide from *Sargassum fusiforme*

Jinhong Hu [a,b], Wanzi Yao [a,b], Shiyuan Chang [a,b], Lijun You [a,b,*], Mouming Zhao [a,b], Peter Chi-Keung Cheung [c], Kseniya Hileuskaya [d]

[a] School of Food Science and Engineering, South China University of Technology, Guangzhou, Guangdong 510640, People's Republic of China
[b] Research Institute for Food Nutrition and Human Health (111 Center), Guangzhou, Guangdong 510640, People's Republic of China
[c] Food & Nutritional Sciences Program, School of Life Sciences, Chinese University of Hong Kong, Hong Kong 999077, People's Republic of China
[d] Institute of Chemistry of New Materials, National Academy of Sciences of Belarus, Skaryna str., Minsk 220141, Belarus

ARTICLE INFO

Keywords:
Sargassum fusiforme
Algal polysaccharide
Structural characteristics
Anti-photoaging
UVB irradiation

ABSTRACT

In this study, a purified algal polysaccharide (P1) was isolated from *Sargassum fusiforme* and its structural characteristics and anti-photoaging activity were studied. Results showed that P1 had a molecular weight of 289 kDa and was mainly composed of mannuronic acid, guluronic acid and fucose with molar ratio of 7.67:2.35:1.00. The backbone of P1 was →4)-*β*-ManA-(1→4)-*α*-GulA-(1→4)-*β*-ManA-(1→4)-*β*-ManA-(1→4)-*α*-GulA-(1→4)-*β*-ManA-(1→3,4)-*β*-ManA-(1→ with a terminal group of *α*-Fuc*p*-(1→ linked to O-3 position of →3,4)-*β*-ManA-(1→. In addition, P1 could inhibit the expressions of MMPs (MMP-1, MMP-3 and MMP-9) in the UVB-irradiated HaCaT cells, indicating that P1 could reduce collagen loss caused by UVB irradiation. It also reduced the contents of ROS and inflammatory factors (TNF-*α*, IL-6 and IL-1*β*), indicating that P1 could reduce the oxidative stress and inflammation response. Thus, *Sargassum fusiforme* polysaccharide P1 could be used as a potential functional food to relieve skin photoaging.

1. Introduction

Human skin is the largest defense organ capable of performing complex functions. It resists outside pathogenic microorganisms, radiation and harmful chemical agents (Michalak et al., 2021). Skin photoaging is currently one of the most serious dermatological and cosmetic problems (Rigel, 2008) and the main cause of exogenous skin aging (Wen et al., 2016). Studies demonstrated that UVB could cause wrinkles, non-melanoma, oxidative stress, inflammation, DNA damage cancer and other damages (Kwon et al., 2019). UVB mainly degrades type I collagen and inhibits its production by enhancing the expression of matrix metalloproteinases (MMPs) including collagenase (MMP-1), stromelysin (MMP-3) and gelatinase (MMP-9) (Xiao et al., 2020). In addition, excessive UVB radiation could cause a large accumulation of reactive oxygen species (ROS) (Youn et al., 2014). Besides, UVB could activate MAPK pathway with a high level of ROS and up-regulate the production of activating protein-1 (AP-1) which mainly leads to the massive expression of MMPs (Duan et al., 2019). Moreover, UVB could also directly activate NF-κB pathway, produce vast inflammatory factors (TNF-*α*, IL-6 and IL-1*β*, etc.), up-regulate the expression of MMP-9 and finally lead to skin photodamage (Auh & Madhavan, 2021).

Human immortalized epidermal cells (HaCaT) cells are keratinocytes located in the epidermal layer of the skin (Masaki et al., 2009). Their growth state can reflect the health status of the skin. Therefore, we can evaluate the photodamage and the healing of the skin by determining the changes of MMPs (MMP-1, MMP-3 and MMP-9), reactive oxygen species (ROS), inflammatory factors (TNF-*α*, IL-6 and IL-1*β*) contents in HaCaT cells.

Many studies indicated that dietary supplements such as polysaccharides (Ji et al., 2017), polyphenols (Filip et al., 2011), collagen peptides (Ye et al., 2018), anthocyanins (Zhi et al., 2020), sterols (Misawa et al., 2017), ursolic acid (Son & Lee, 2020), and piperine (Verma et al., 2017) had potential anti-photoaging activity to maintain skin health. Polysaccharides such as fucoidan isolated from *Hizikia fusiforme* (Wang et al., 2020), mushroom polysaccharide extracted from *Tremella fuciformis* (Wen et al., 2016), and bacterial exopolysaccharides produced by *Lactobacillus plantarum* HY7714 (Lee et al., 2021) have been demonstrated to exhibit strong anti-photoaging activity.

* Corresponding author at: School of Food Science and Engineering, South China University of Technology, 381 Wushan Road, Guangzhou 510640, People's Republic of China.
E-mail address: feyoulijun@scut.edu.cn (L. You).

https://doi.org/10.1016/j.foodres.2022.111267
Received 21 March 2022; Received in revised form 15 April 2022; Accepted 17 April 2022
Available online 20 April 2022
0963-9969/© 2022 Elsevier Ltd. All rights reserved.

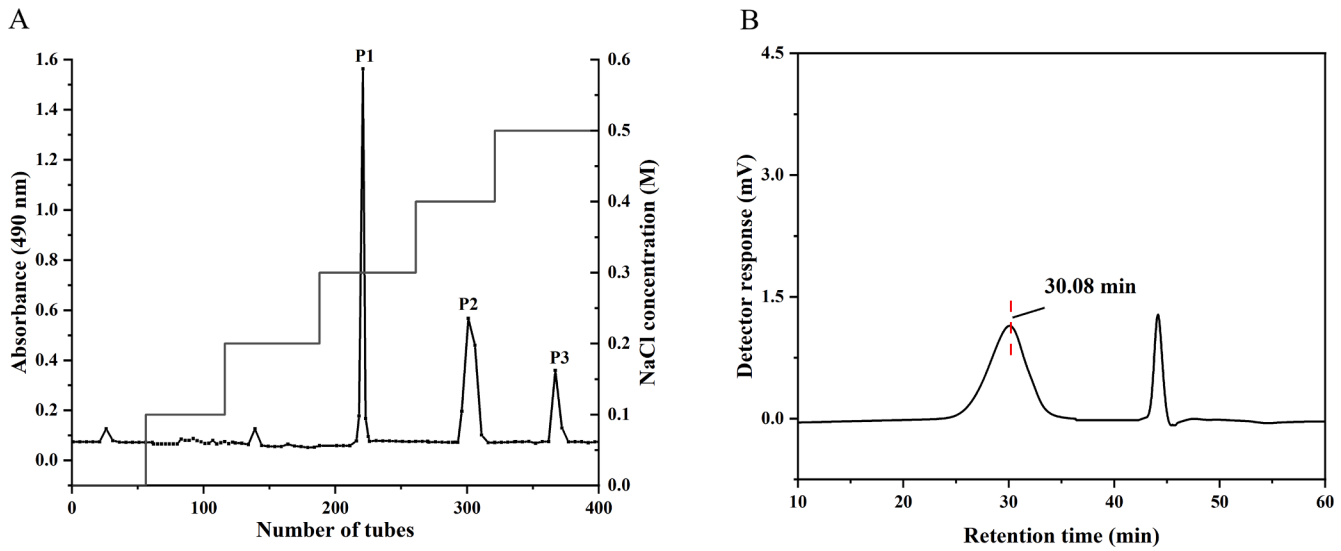

Fig. 1. Elution curve of *Sargassum fusiforme* polysaccharide (A) and HPGPC molecular weight distribution of purified *Sargassum fusiforme* polysaccharide P1 (B).

Table 1
Molecular weights and chemical compositions of P1.

Samples	P1
Mw (kDa)	289
Chemical compositions	
Protein (%)	0.68 ± 0.04
Total carbohydrate (%)	20.73 ± 0.05
Reducing sugar (%)	3.60 ± 0.24
Uronic acid (%)	74.04 ± 1.86
Sulfate (%)	1.00 ± 0.05
Monosaccharide composition (molar ratio)	
Fuc	1.00
GulA	2.35
ManA	7.67

Algal polysaccharide is favored by people because of its wide source, low toxicity and various biological activities (Sanjeewa et al., 2017; Shao et al., 2020). *Sargassum fusiforme* is a pharmaceutical or edible alga that is rich in polysaccharides. Reports have shown that *Sargassum fusiforme* polysaccharides are mainly composed of fucoidan and alginic acid with laminaran as minor component (Zhang et al., 2020). It plays a vital role in antioxidant (Nie et al., 2021), anti-inflammatory (Chen et al., 2021), hypoglycemic (Li et al., 2021) and other aspects. In our previous study, a crude algal polysaccharide isolated from *Sargassum fusiforme* has been proved to exhibit strong anti-photoaging activity by increasing SOD and GSH-Px enzyme activities and inhibiting ROS, MMP-1 and MMP-9 productions in UVB-induced HaCaT cells (Ji et al., 2017).

In the present study, a fraction of this *Sargassum fusiforme* polysaccharide was purified and its precise structure was elucidated by high-performance gel permeation chromatography (HPGPC), Fourier transform infrared spectroscopy (FT-IR), ion chromatography (ICS), scanning electron microscope (SEM), gas chromatography-mass spectrometer (GC–MS) and nuclear magnetic resonance spectroscopy (NMR). Then, the anti-photoaging activity of the purified polysaccharide fraction (denoted as P1) was evaluated by determining the expressions of MMPs (including MMP-1, MMP-3 and MMP-9), ROS and inflammatory factors (TNF-α, IL-6 and IL-1β) in UVB-induced HaCaT cells. The results of this study would provide insight for the preparation of algal polysaccharides with potential applications in anti-photoaging functional foods.

2. Materials and methods

2.1. Materials and reagents

Sargassum fusiforme was collected from Dongtou District, Wenzhou, Zhejiang, China in May 2019. The DEAE Sepharose fast-flow was purchased from GE Company (Fairfield, Connecticut, USA). Hydrochloric acid, concentrated sulfuric acid, NaCl and phenol were purchased from the Guangzhou Chemical Reagent Factory (Guangzhou, Guangdong, China). The monosaccharide standards (Fuc, Ara, Gal, Glc, Xyl, Fru, Rib, GalA, GlcA, ManA and GulA) and the dextran standards with different molecular weights (4.32, 12.6, 126, 289 and 496 kDa) were purchased from Sigma-Aldrich (St Louis, MO, USA). The HaCaT cells (human immortalized keratinocytes) were purchased from the Cell Resource Center of Shanghai Academy of Biological Sciences (Shanghai, China). The MEM medium was purchased from Biosharp Biotechnology Co., Ltd. (Hefei, Anhui, China). The MTT kit was purchased from Nanjing Jiancheng Bioengineering Institute Co., Ltd. (Nanjing, Jiangsu, China). The MMP-1 and MMP-9 ELISA kits were purchased from Neobioscience Technology Co., Ltd. (Shenzhen, Guangdong, China). The MMP-3, TNF-α, IL-6 and IL-1β ELISA kits were purchased from Multi Sciences (Lianke) Biotech Co., Ltd. (Hangzhou, Zhejiang, China). The reactive oxygen species (ROS) assay kit and diethyl pyrocarbonate (DEPC) water were purchased from Beyotime Biotechnology Co., Ltd. (Nanjing, Jiangsu, China). Trizol reagent, reverse transcription (RT) kit and qRT-PCR kit were purchased from Thermo Fisher Scientific Co., Ltd. (Austin, Texas, USA).

2.2. Extraction and purification of polysaccharides from Sargassum fusiforme

Sargassum fusiforme polysaccharide was extracted using the method reported in our previous study with some modifications (Chen et al., 2021). Ultrafine pulverization (XDW6-BI, Dawei Machinery Co., Ltd., Jinan, Shandong, China) was used to produce superfine powder of *Sargassum fusiforme* for increasing the extraction yield of crude polysaccharide. The algal powder was decolorized by 95% ethanol for 4 h (1:4, w/v, 3 times). Then the decolorized powder was extracted with water at 100 °C for 4 h (1:50, w/v), filtered, centrifuged at 8000 r/min for 15 min and concentrated to 1/10 of the original volume. Then the supernatant was precipitated by 80% ethanol overnight and lyophilized to obtain *Sargassum fusiforme* crude polysaccharide.

Sargassum fusiforme crude polysaccharide was purified by DEAE

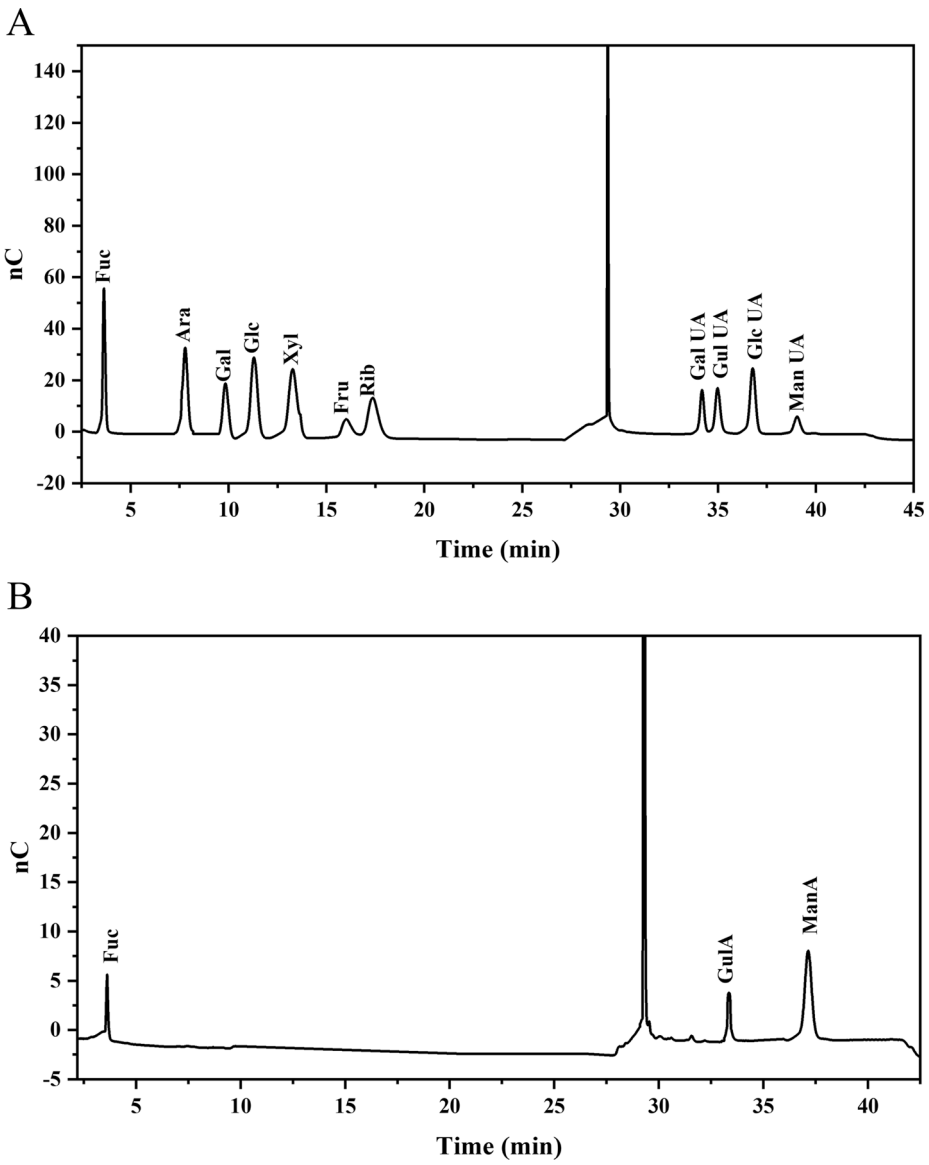

Fig. 2. Ion chromatographic curve of standards (A) and monosaccharide composition ion chromatogram of P1 (B). The monosaccharide standards from left to right are fucose, arabinose, galactose, glucose, xylose, fructose, ribose, galacturonic acid, gulonuronic acid, glucuronic acid, and mannuronic acid.

Sepharose fast flow column. Gradient elution was performed with 0, 0.1, 0.2, 0.3, 0.4 and 0.5 M NaCl at a flow rate of 2.0 mL/min using a BT100-2 pump (Baoding Qili Peristaltic Pump Co., Ltd., Baoding, Hebei, China). An aliquot of the eluent was taken every 5 min and determined at 490 nm by the phenol sulfuric acid method.

The 0.3 M NaCl eluted component was chosen and then dialyzed and lyophilized to obtain P1 for further study.

2.3. Structural characterization of P1

2.3.1. Molecular weight

High-performance gel permeation chromatography (HPGPC) was used to determine the molecular weight of the purified fraction P1 with a binary HPLC pump (Waters 1525, Waters Co., Ltd., Milford, USA) and a Waters 2414 differential refraction detector. TSK G6000 PWXL column (7.8 mm × 300 mm i.d., 13 μm, Tosoh Co., Ltd., Tokyo, Japan) and TSK G3000 PWXL column (7.8 mm × 300 mm i.d., 7 μm, Tosoh Co., Ltd.) were connected in series at 35 ± 0.1 °C. A 25 μL of sample was injected into each frame at a flow rate of 0.5 mL/min and 0.02 M KH_2PO_4 was used as the mobile phase. The dextrans with different molecular weights (4.32, 12.6, 126, 289 and 496 kDa) were used as standards.

2.3.2. Chemical compositions

The total sugar content was determined by the phenol-sulfuric acid method with fucose as the standard (Dubois et al., 1956). The reducing sugar content was determined by the 3,5-dinitrosalicylic acid (DNS) method with fucose as the standard (Lindsay, 1973). The sulfuric acid content was determined by the barium sulfate turbidimetric method with K_2SO_4 as the standard (Zhang et al., 2015). The uronic acid content was determined by the m-hydroxyl diphenyl assay with mannuronic acid as the standard (Nelly & Gustav, 1973).

2.3.3. Monosaccharide composition

The monosaccharide composition of P1 was analyzed by ion chromatography (ICS5000, Thermo Fisher Scientific Co., Ltd., MA, USA) (Wang et al., 2018). The sample was hydrolyzed in 2 M trifluoroacetic acid (TFA) at 105 °C for 6 h. After cooling to room temperature, the mixture was dried at 60 °C under reduced pressure. Chromatographic methanol (4 mL × 5) was added and evaporated. The product was dissolved in 2 mL deionized water and determined after passing through a

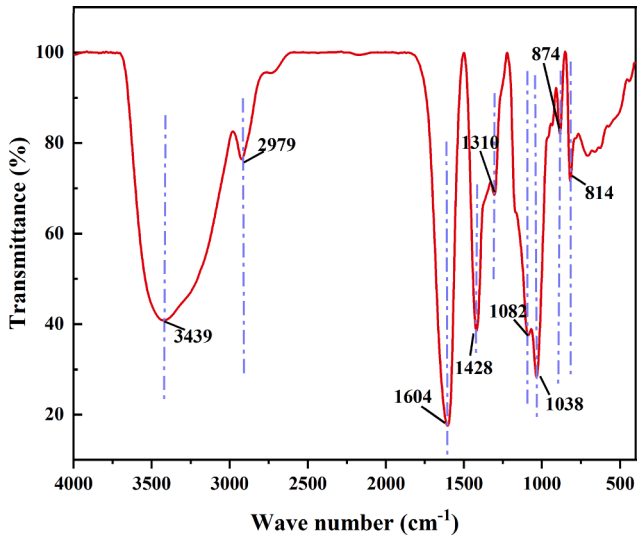

Fig. 3. FT-IR spectra of P1.

Table 2
GC–MS data for methylation analysis of P1.

Methylated sugar	Linkage type	Molar ratio (%)	Mass fragments (*m/z*)
→4)-Man*p*-(1→	1,4,5-tri-O-acetyl-2,3,6-tri-O-methyl mannitol	44.97	73, 87, 102, 118, 162, 175, 205, 235, 279
Man*p*-(1→	1,5-di-O-acetyl-2,3,4,6-tetra-O-methyl mannitol	17.52	73, 87, 102, 118, 162, 189, 235
→3,4)-Man*p*-(1→	1,3,4,5-tetra-O-acetyl-2,6-di-O-methyl mannitol	7.89	59, 71, 101, 129, 161, 191, 207
Fuc*p*-(1→	1,5-di-O-acetyl-6-deoxy-2,3,4-tri-O-methyl fucitol	8.28	69, 91, 102, 118, 134, 162, 176
→4)-Gul*p*-(1→	1,4,5-tri-O-acetyl-2,3,6-tri-O-methyl gulitol	21.34	59, 71, 101, 129, 161, 189, 262

0.22 μm membrane.

Dionex™ CarboPac™ PA10 (250 × 4.0 mm, 10 μm) liquid chromatography column was used to detect the monosaccharide component at a flow rate of 0.5 mL/min. An injection volume of 5 μL was used to each run at 30 °C. Mobile phase A was 0.1 M NaOH, the mobile phase B was 0.1 M NaOH and 0.2 M NaAc.

2.3.4. Fourier transform infrared spectroscopy (FT-IR)

The Fourier transform infrared spectroscopy was performed on a Tensor 27 infrared spectrometer (Bruker Co., Ltd., Bergisch Gladbach, Germany). The sample and KBr particles were grounded into powder with a mortar and determined in the range of 400–4000 cm^{-1} (Chen et al., 2020).

2.3.5. Methylation analysis of P1

The methylation method was modified according to Liu and others (Liu, 2014). About 10 mg P1 was dissolved in H_2O, then 1 mL 100 mg/mL carbodiimide was added for the reduction reaction. Two hours later, after adding 1 mL 2 M imidazole, the uronic acid of P1 was reduced with 1 mL 30 mg/mL $NaBD_4$. After 3 h, 100 μL of glacial acetic acid was added to terminate the reaction. Next, the solution was lyophilized after 48 h of dialysis and dissolved in 500 μL DMSO for methylation. Subsequently, the sample was incubated with 1 mg NaOH for 30 min and then methylated with 50 μL CH_3I for 1 h. Then 1 mL water was added to terminate the reaction, the mixture was extracted by CH_2Cl_2 (2 mL × 3). The water phase was abandoned. After the CH_2Cl_2 phase was evaporated, TFA (100 μL, 2 M) was added, and the solution was hydrolyzed at 121 °C for 90 min and dried. In the system, ammonia (50 μL, 2 M) and $NaBD_4$ (50 μL, 1 M) were added and stirred for 2.5 h at room temperature. The reaction was terminated by 20 μL acetic acid. The product was dried with N_2, washed twice with 250 μL methanol, and then dried with N_2. Acetylation was performed with 250 μL acetic anhydride at 100 °C for 2.5 h. Then 1 mL water was added to terminate the reaction. The extraction step was repeated with CH_2Cl_2 (2 mL × 3). The final CH_2Cl_2 phase was analyzed by GC–MS (Agilent 7890A-5977B, Agilent Technologies Inc., Santa Clara, CA, USA) at 30–600 (*m/z*). An injection volume of 1 μL was used for each run. The injector temperature was kept at 230 °C and helium was used as carrier gas.

2.3.6. NMR analysis

A nuclear magnetic resonance spectrometer (600 M AVANCE II, Bruker Technology Co., Ltd., Bergisch Gladbach, Germany) was used to identify P1′s structure. About 50 mg of P1 was repeatedly lyophilized in 99.9% D_2O to completely replace H by D. Finally, 0.55 mL D_2O was added and transferred to a 5 mm NMR tube. One-dimensional NMR (^1H and ^{13}C spectrum) and two-dimensional NMR (homonuclear $^1H/^1H$ correlation COSY spectrum, heteronuclear $^1H/^{13}C$ single quantum coherent HSQC spectrum and heteronuclear $^1H/^{13}C$ multi-bond coherent HMBC spectrum) were analyzed to identify P1′s structure.

2.4. Anti-photoaging activity of P1

2.4.1. Cell culture

Human immortalized keratinocytes HaCaT cells were cultured in MEM medium containing 10% (v/v) FBS and 1% (v/v) penicillin & streptomycin (antibiotics), in a 5% CO_2 incubator at 37 °C (Thermo Scientific Forma 3111, MA, USA).

2.4.2. Cell cytotoxicity of P1

The cells were added to a 96-well plate and cultured for 24 h. Subsequently, the culture medium was discarded, and 0, 31.25, 62.5, 125, 250 μg/mL P1 and 31.25 μg/mL the positive control hyaluronic acid (HA, Macklin Biochemical Co., Ltd, Shanghai, China) (Sun et al., 2017) were added and cultured for 24 h. The MTT kit (Nanjing Jiancheng Bioengineering Institute Co., Ltd., Nanjing, Jiangsu, China) was used to determine the survival rate of cells, and the experimental safe concentration was chosen based on the survival rate.

2.4.3. Determination of MMP-1, MMP-3, MMP-9, TNF-α, IL-1β and IL-6 levels

HaCaT cells were spread on a 24-well plate at a concentration of 2×10^5 cells/well and cultured for 24 h. Then the culture medium was discarded, an equal volume of PBS was added, and the HaCaT cells were irradiated with a UVB illuminator (HOPE-MED 8140B, Teda Hepu Industry & Trade Co., Ltd., Tianjin, China) at 9 mJ/cm^2, the control group was treated with aluminum foils for shading. After that, 31.25, 62.5, 125 μg/mL of P1 and 31.25 μg/mL HA were added and cultured for 24 h. The cell suspension was collected and centrifuged, the supernatant was taken, and the contents of MMP-1, MMP-3, MMP-9, TNF-α, IL-1β and IL-6 were determined by commercial kits according to the methods provided by the manufacturers. The MMP-1 and MMP-9 ELISA kits were purchased from Neobioscience Technology Co., Ltd. (Shenzhen, Guangdong, China). The MMP-3, TNF-α, IL-6 and IL-1β ELISA kits were purchased from Multi Sciences (Lianke) Biotech Co., Ltd. (Hangzhou, Zhejiang, China). The reactive oxygen species (ROS) assay kit was purchased from Beyotime Biotechnology Co., Ltd. (Nanjing, Jiangsu, China).

2.4.4. Determination of ROS levels

The cells were spread to a 96-well black plate and cultured for 24 h. Then the culture medium was discarded. An equal volume of PBS was added. And the HaCaT cells were irradiated with a UVB illuminator at 9 mJ/cm^2, the control group was treated with aluminum foils for shading. After that, 31.25, 62.5, 125 μg/mL of P1 and 31.25 μg/mL HA were

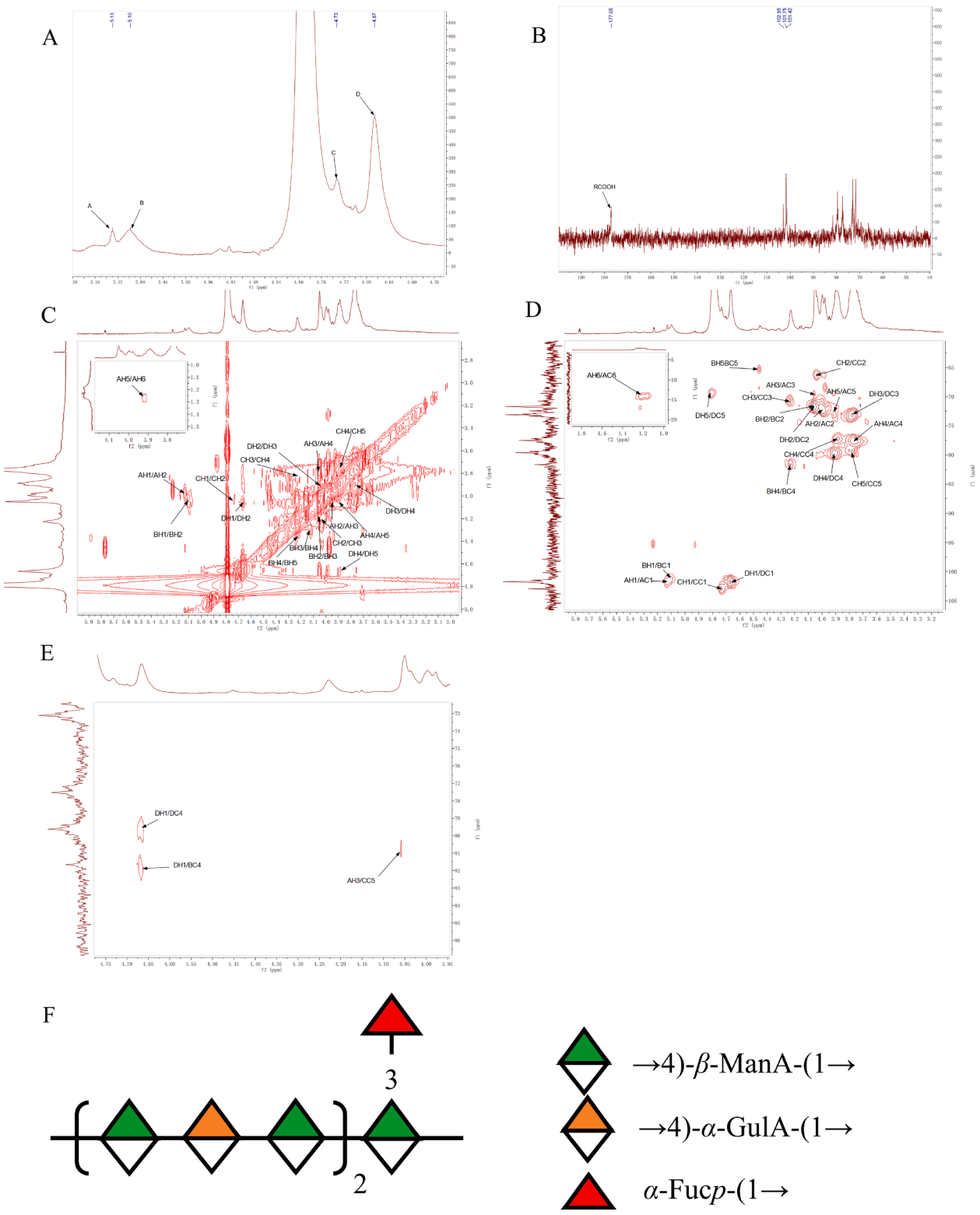

Fig. 4. ^{1}H spectrum (A); ^{13}C spectrum (B); ^{1}H–^{1}H COSY spectrum (C); ^{1}H–^{13}C HSQC spectrum (D); ^{1}H–^{13}C HMBC spectrum (E) and predicted structure (F) of P1.

added and cultured for 24 h. Then the cell supernatant was discarded, and the DCFH-DA probe diluted by 5000 times was added to each well. The black plate was incubated in the cell incubator for 20 min. After that, the wells were washed with MEM (100 μL/well × 3) to remove the excess DCFH-DA probe. A fluorescence microplate reader (Varioskan LUX, Thermo Fisher Scientific Co., Ltd., MA, USA) was used to detect the absorbances at 488 and 525 nm.

2.4.5. Gene expressions of MMPs

Gene expression was analyzed by Quantitative real-time polymerase chain reaction (qRT-PCR). The supernatant was collected. The cells were disrupted with Trizol (1 mL/well). The cDNA was synthesized by the RT kit with gDNA clean. The T100^{TM} Thermal Cycler (Bio-Rad Laboratories, Berkeley, California, USA) was used to reverse the transcription of mRNA. The SYBR^{TM} Green Master Mix was used for qRT-PCR workflows.

Table 3
Chemical shifts of P1 in ^{1}H and ^{13}C NMR spectra.

Sugar residue	H1/C1	H2/C2	H3/C3	H4/C4	H5/C5	H6/C6
A *α*-Fuc*p*-(1→	5.13/101.75	3.99/72.04	4.06/69.38	3.78/77.56	3.91/73.26	1.22/14.22
B→4)-*α*-GulA-(1→	5.11/101.17	4.04/71.48	4.16/71.77	4.25/81.87	4.46/65.27	-/177.05
C→3,4)-*β*-ManA-(1→	4.74/102.93	4.04/66.10	4.23/70.84	3.88/74.24	3.78/79.40	-/177.05
D→4)-*β*-ManA-(1→	4.63.101.72	4.06/71.70	3.78/73.41	3.91/79.72	4.80/69.65	-/177.05

The amplification conditions were set at 95 °C for 2 min, and 40 cycles at 95 °C for 15 s, 60 °C for 1 min. The sequences of the specific primers used in qRT-PCR were listed in **Table S1**. The relative transcript levels of target genes were normalized with *β*-actin and calculated via $2^{-\Delta\Delta Ct}$ method.

2.5. Statistical analysis

Statistical analysis of the data was carried out using IBM SPSS Statistics 26 analysis software (IBM Co., Ltd., Chicago, USA). The experimental data were expressed as mean ± standard deviation ($\bar{x}\pm SD$) ($n \geq 3$). Different letters indicated a statistically significant difference ($p < 0.05$). The LSD test methods were used for pairwise comparison. Statistical analysis was carried out by ANOVA test.

3. Results and discussion

3.1. Structural characteristics of P1

3.1.1. The molecular weight and chemical composition of P1

In this study, the crude *Sargassum fusiforme* polysaccharide was purified by DEAE Sepharose fast flow column and eluted by NaCl solutions with different concentrations. According to the DEAE elution profile (Fig. 1**A**), there were three main components occurred at the 0.3, 0.4 and 0.5 M NaCl elution gradient, which were named P1, P2 and P3, respectively. The yields of P1, P2 and P3 were 36.47, 6.11 and 1.36%, respectively. The yield of P1 was higher yield than the one (16.61%) previously reported (Ji et al., 2017). Since fraction P1 eluted with 0.3 M NaCl showed higher anti-photoaging activity (data not shown) so it was selected for the following experiments.

According to the HPGPC profile (Fig. 1**B**), a symmetric wide peak appeared at the retention time of 30.08 min, indicating that the average molecular weight of P1 was 289 kDa (Table 1). There was only one symmetrical wide peak in front of the solvent peak, thus P1 was a relatively pure component to determine the precise structure. Polysaccharides with high molecular weight such as fucoidan have been reported to have strong antioxidant and anti-photoaging activities (Wang et al., 2020) probably via direct scavenging free radicals (Penna et al., 2019), regulating the intestinal flora (Kong et al., 2021), binding to certain receptors which regulate the expressions of related proteins (Lee et al., 2021; Wang et al., 2020) or regulating the activities of related enzymes *in vivo* (Wen et al., 2016). The contents of total carbohydrate and uronic acids of P1 were 20.73 and 74.04%, respectively, with very low level of sulfate group and protein. Therefore, P1 was dominant by uronic acids.

According to the ion chromatography results (Fig. 2 and Table 1), P1 was mainly composed of mannuronic acid, guluronic acid and fucose at a molar ratio of 7.67:2.35:1.00 (Table 1). Previous reports showed that alginate was one of the common polysaccharides in *Sargassum fusiforme*. Alginate was composed of M (*β*-D-mannouronic acid), G (*α*-L-guronuronic acid) with the MG fractions in different proportions (Li et al., 2018). Therefore, alginate was the main polysaccharide component of P1.

3.1.2. FT-IR spectra analysis of P1

According to Fig. 3, the wavelengths of 3439, 2928, and 1604 cm^{-1} were characteristic peaks corresponding to the O-H, C-H and COO– stretching vibration of sugars intermolecular or intramolecular, respectively (Chang et al., 2021). The wavelength at 1428 cm^{-1} was the symmetric stretching vibration of COO– (Zhang et al., 2019). The wavelength of 1038 cm^{-1} was the stretching vibration of the C-OH side group. The region between 800 and 1200 cm^{-1} was considered a fingerprint region due to its ability to reflect the vibrations of the sugar ring (Wang et al., 2020). The wavelength at 814 cm^{-1} was corresponding to the *α*-linked glycosyl residue (Li et al., 2020). The two weak peaks with wavelengths of 1310 cm^{-1} and 1082 cm^{-1} consisted the stretching vibration of C-O-C glycoside (Crispin et al., 2019). The peak at 874 cm^{-1} was the characteristic peak corresponding to the vibration of the *β* isomer (Xie et al., 2021). The results of FT-IR showed that P1 had a typical polysaccharide structure with uronic acid and *α* as well as *β* linked glycosyl residue. The content of impurities such as the sulfate group was low.

3.1.3. Analysis of glycosidic bond types of P1

The methylation of P1 was identified by GC–MS (Table 2) and the fragment ions mass spectra are shown in **Figure S1**. According to the database (Sanshu Biotechnology Co., Ltd., Shanghai, China), P1 mainly consisted of →4)-Man*p*-(1→ (44.97%), Man*p*-(1→ (17.52%), →3,4)-Man*p*-(1→ (7.89%), Fuc*p*-(1→ (8.28%) and →4)-Gul*p*-(1→ (21.34%) (Table 2). It was found that the 1,4-linked mannose and gulose residues were the dominant major building blocks of P1. What's more, t-Man*p* and t-Fuc*p* were the terminal residues of P1, and 1,3,4-linked mannose residue was the branch of P1.

Combined with the uronic acid content and monosaccharide composition results, →4)-Man*p*-(1→, →4)-Gul*p*-(1→, Man*p*-(1→ and →3,4)-Man*p*-(1→ might be corresponding to →4)-ManA-(1→, →4)-GulA-(1→, ManA-(1→ and →3,4)-ManA-(1→, respectively.

Since the information on guluronic acid was not included in the GC–MS database, guluronic acid could not be identified in the results. However, ion chromatography results indicated that there was guluronic acid in P1 with a molar ratio of 21.34% (Fig. 2**B**). The molar ratio of *t*-Man*p* (17.52%) was higher than actual one (9.84%). This may be because the acid treatment in the methylation process removed some of the →4)-Man*p*-(1→ resulting with free glycosidic bonds which were not removed during dialysis (Liu, Ye et al., 2021).

3.1.4. NMR analysis of P1

Nuclear magnetic resonance spectrum NMR is increasingly used for the structural analysis of polysaccharides. The configuration of polysaccharide carbon, the sequence of sugar chain and the proportion of polysaccharide residue can be further characterized by 1D NMR (^{1}H NMR and ^{13}C NMR) and 2D NMR (^{1}H–^{1}H COSY, ^{1}H–^{13}C HSQC, ^{1}H–^{1}H TCOSY and ^{1}H–^{13}C HMBC).

In this study, 1D (^{1}H and ^{13}C) and 2D (COSY and HSQC) NMR spectra of P1 were used to assign the ^{1}H and ^{13}C chemical shifts for sugar residues (Fig. 4**A-D**). H/C chemical shifts in all sugar residues were fully assigned on basis of NMR spectra and literature data. Based on the results of ^{13}C NMR (Fig. 4**B**), the peak at *δ* 177.05 ppm indicated the presence of uronic acids which was consistent with monosaccharide composition.

Two-dimensional homonuclear ^{1}H–^{1}H COSY spectrum is used to analyze the relevant information between adjacent hydrogen atoms in the same carbon atom. Generally, it is J3 coupling between adjacent protons, and the peak on the diagonal corresponds to the one-dimensional ^{1}H spectrum. Two-dimensional heteronuclear ^{1}H–^{13}C HSQC spectrum is used to analyze the ^{1}H and ^{13}C distribution of direct coupling (^{1}J) in the same glycosidic bond (Shi et al., 2021). According to the ^{1}H–^{13}C HSQC (Fig. 4**D**), the anomeric signals of 4 kinds of glycosidic

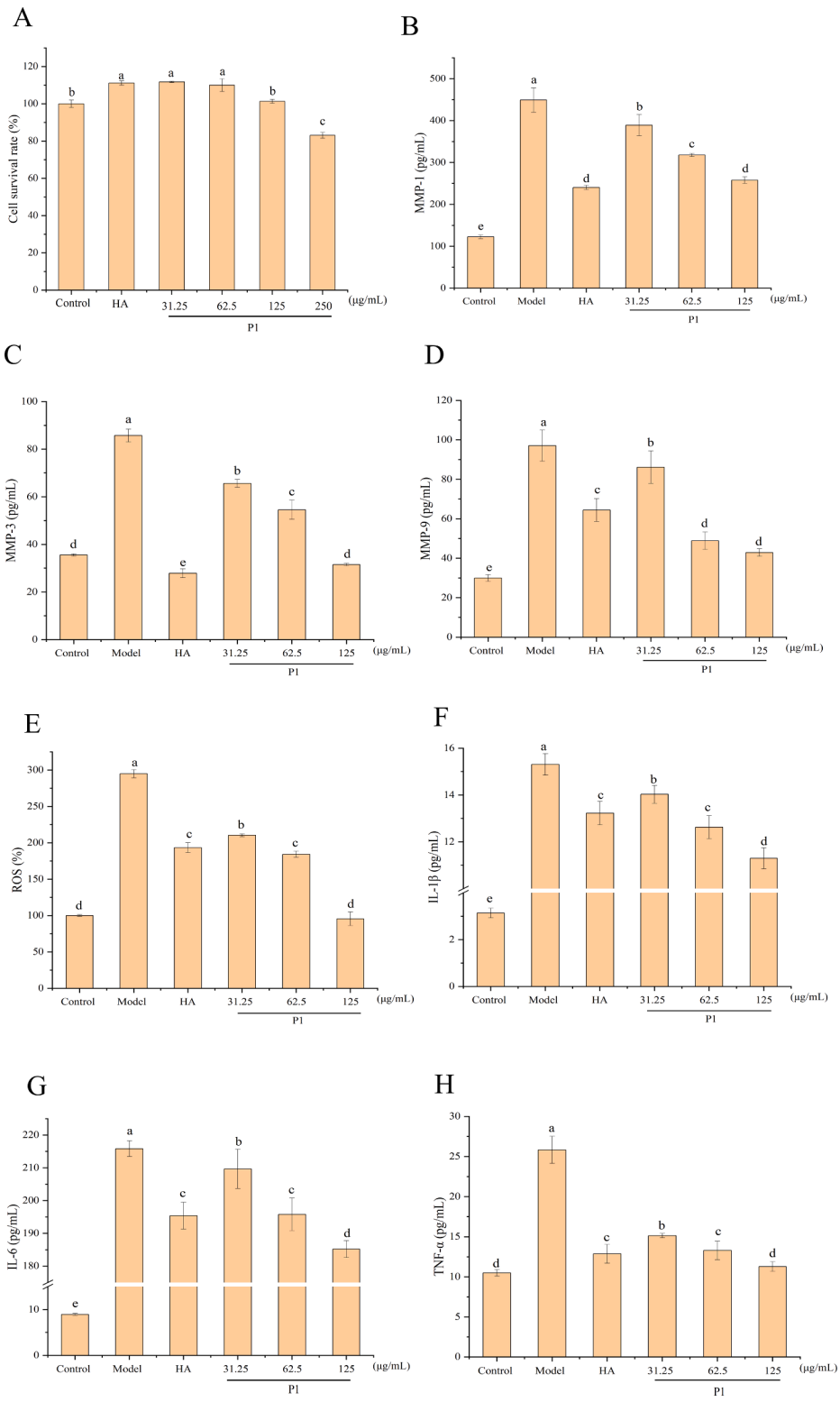

Fig. 5. Effects of P1 on sample toxicity (A) and the content of MMP-1 (B); MMP-3 (C); MMP-9 (D); ROS (E); IL-1β (F); IL-6 (G) and TNF-α (H) in HaCaT cells after UVB radiation. Different letters represented significant differences ($p < 0.05$).

bonds were marked in the signal interval of anomeric hydrogen and anomeric carbon, which were labeled as glycosidic bonds A, B, C and D, respectively. The anomeric signals of A and B (δ 5.13/101.75 and 5.11/101.17 ppm) belong to the α configuration, while the anomeric signals of C and D (δ 4.74/102.93 and 4.63/101.72 ppm) belong to the β configuration (Cui, 2005). Taking the glycosidic bond A as an example, according to the H-1 signal in the HSQC spectrum, the corresponding H-2 (δ 3.99 ppm) was found in the COSY spectrum (Fig. 4**C**). According to the H-2 signal in COSY spectrum, the coupled carbon signal C-2 (δ 72.04 ppm) was found in HSQC spectrum. According to the COSY and HSQC spectra, the corresponding H-3/C-3–H-6/C-6 were found in a one-to-one correspondence, which were δ 4.06/69.38, 3.78/77.56, 3.91/73.26 and

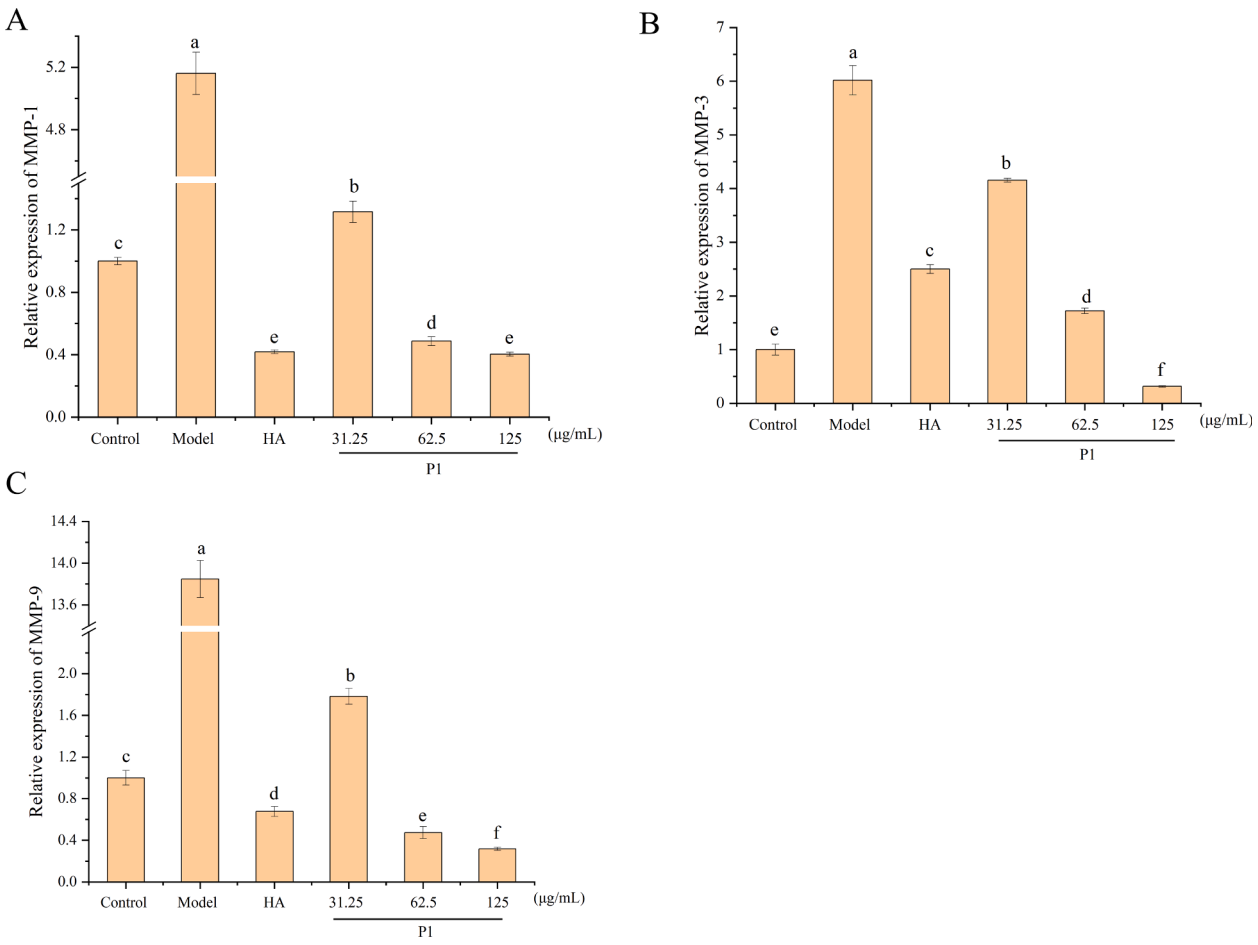

Fig. 6. Effects of P1 on MMP-1 (A); MMP-3 (B) and MMP-9 (C) mRNA relative expression in HaCaT cells after UVB radiation. Different letters represented significant differences ($p < 0.05$).

1.22/14.22 ppm, respectively. Combined with the references and methylation results, it was speculated that the glycosidic bond A might be *α*-Fuc*p*-(1→ (Cheng et al., 2021). The chemical shifts of H-2/C-2–H-5/C-5 of B, C and D were marked in the same way as A, and the detailed chemical shifts ^{1}H and ^{13}C signals were shown in Table 3. The H-2/C-2–H-5/C-5 of B were *δ* 4.04/71.48, 4.16/71.77, 4.25/81.87 and 4.46/65.27 ppm, respectively. The H-2/C-2–H-5/C-5 of C were *δ* 4.04/66.10, 4.23/70.84, 3.88/74.24 and 3.78/79.40 ppm, respectively. The H-2/C-2–H-5/C-5 of D were *δ* 4.06/71.70, 3.78/73.41, 3.91/79.72 and 4.80/69.65 ppm, respectively.

Combined with the corresponding references and methylation results, it was inferred that the glycosidic bonds B, C and D were →4)-*α*-GulA-(1→, →3,4)-*β*-ManA-(1→ and →4)-*β*-ManA-(1→ (Cong et al., 2014; DeRamos et al., 1997; Holtan et al., 2006; Youssouf et al., 2017). The carbonyl group of uronic acid is generally located at C-6, thus the C-6 signals of →4)-*α*-GulA-(1→, →3,4)-*β*-ManA-(1→ and →4)-*β*-ManA-(1→ were marked as *δ* 177.05 ppm, and the active hydrogens H-6 were not shown in the COSY spectrum.

The ^{1}H–^{13}C HMBC spectrum shows carbon-hydrogen coupling between different sugar residues (Hao et al., 2019). According to the HMBC spectrum results of P1 (Fig. 4**E**), the cross-peaks of D H1/D C4 (*δ* 4.67/79.19 ppm) and D H1/B C4 (*δ* 4.67/81.92 ppm) explained the O-1 of D was attached to the C-4 of D and B. It indicated that the glycosidic bond B and D are both 1,4-linked configurations, which further proved that the glycosidic bonds B and D were →4)-*α*-GulA-(1→ and →4)-*β*-ManA-(1→, respectively. The cross-peak of A H3/C C5 (*δ* 4.06/80.78 ppm) showed that *α*-Fucp-(1→ might be linked to →3,4)-*β*-ManA-(1→ at the O-3 position.

The exact structure of P1 was inferred from the methylation results and HMBC spectrum (Fig. 4**F**). The backbone of P1 was →4)-*β*-ManA-(1→4)-*α*-GulA-(1→4)-*β*-ManA-(1→4)-*β*-ManA-(1→4)-*α*-GulA-(1→4)-*β*-ManA-(1→3,4)-*β*-ManA-(1→, and the terminal group *α*-Fuc*p*-(1→ was linked to the main chain via O-3 position of →3,4)-*β*-ManA-(1→. The results showed that P1 may be a typical alginic acid (M/G was about 2.5) with a long main chain and few branches. Some peaks in the ^{1}H spectrum of P1 were not completely separated, and the signals of the HMBC spectrum were weak, which might be caused by the large molecular weight of P1.

3.2. *The anti-photoaging activity of P1*

Matrix metalloproteinase (MMP) is a group of enzymes responsible for the degradation of extracellular matrix with more than 25 kinds, including collagenase (MMP-1), stromelysin (MMP-3) and gelatinase (MMP-9) and so on (Benbow & Brinckerhoff, 1997). Ultraviolet irradiation activates NF-κB, which stimulates the secretion of IL-1*β*, IL-6, TNF-*α* and MMPs (Helfrich et al., 2008). The overexpression of MMPs will stimulate the secretion of ROS and accelerate the oxidative damage of skin (Cao et al., 2020; Wen et al., 2020). In our study, the anti-photoaging activity of P1 was determined by using a UVB-induced HaCaT cells model. P1 did not have toxic on HaCaT cells at 0–250 μg/mL. Concentrations of 31.25, 62.5 and 125 μg/mL were set as low, medium and high doses in the following tests (Fig. 5**A**), respectively. After UVB irradiation, the secretion levels of MMP-1, MMP-3, MMP-9, ROS, IL-1*β*, IL-6 as well as TNF-*α* in the model group were all significantly higher than those in the control group, indicating that the model

was set up successfully. Furthermore, P1 could inhibit the productions of MMPs (MMP-1, MMP-3 and MMP-9) in the UVB-irradiated HaCaT cells in a dose-dependent manner (Fig. 5**B-H**), indicating that P1 could reduce collagen loss caused by UVB irradiation. It also reduced the contents of ROS and inflammatory factors (TNF-α, IL-6 and IL-1β), indicating that P1 could reduce the oxidative stress and inflammation response. Moreover, after high dose treatment of P1 (125 μg/mL), the productions of MMPs, ROS and inflammatory factors were significantly lower than those in the positive control group hyaluronic acid (HA). It further suggested that *Sargassum fusiforme* polysaccharide P1 had the potential as an anti-photoaging chemical agent or a functional food.

Effects of fraction P1 on MMPs mRNA relative expression in HaCaT cells after UVB radiation were shown in Fig. 6. After UVB irradiation, the relative mRNA expression levels of MMP-1, MMP-3 and MMP-9 in HaCaT cells were significantly increased. It manifested that the model was successfully established. The relative mRNA expressions of MMP-1, MMP-3 and MMP-9 in UVB-induced HaCaT cells of P1 treated group all decreased in a dose-dependent manner. It was further verified that P1 could effectively inhibit the expression of matrix metalloproteinase. Besides, the relative mRNA expression levels of MMP-3 and MMP-9 in the middle-dose group were lower than those in the positive control HA, and the relative expression of MMP-1 in the high-dose group was close to the positive control HA. All these results demonstrated that P1 could be a good substitute for hyaluronic acid to relieve skin photoaging damage.

In conclusion, P1 might significantly ease or prevent skin photoaging by inhibiting the secretion of MMPs, ROS and inflammatory factors, indicating that P1 had strong anti-photoaging activity.

4. Conclusions

In this study, a polysaccharide P1 was purified from *Sargassum fusiforme*. P1 had a molecular weight of 289 kDa with a carbohydrate content of 20.73% and a uronic acid content of 74.04%, respectively. P1 presented honeycomb pores with little sulfate group. P1 was mainly composed of mannuronic acid, guluronic acid and fucose at a molar ratio of 7.67:2.35:1.00. GC–MS and NMR results showed the backbone of P1 was →4)-β-ManA-(1→4)-α-GulA-(1→4)-β-ManA-(1→4)-β-ManA-(1→4)-α-GulA-(1→4)-β-ManA-(1→3,4)-β-ManA-(1→, and the terminal group α-Fuc*p*-(1→was linked to the main chain via O-3 position of →3,4)-β-ManA-(1→. P1 also exhibited a strong anti-photoaging activity *in vitro* by inhibiting the expressions of MMPs (MMP-1, MMP-3 and MMP-9) and the productions of ROS and inflammatory factors (IL-1β, IL-6 and TNF-α). Our results suggest P1 can be utilized as a potential functional food to prevent skin photoaging.

CRediT authorship contribution statement

Jinhong Hu: Methodology, Data curation, Writing – original draft. **Lijun You:** Supervision. **Wanzi Yao and Shiyuan Chang:** Revision, suggestion. **Mouming Zhao, Peter Chi-Keung Cheung and Kseniya Hileuskaya:** Review and editing.

Declaration of Competing Interest

The authors declare that they have no known competing financial interests or personal relationships that could have appeared to influence the work reported in this paper.

Acknowledgments

The work was funded by National Natural Science Foundation of China (31972011 and 3211101620), Excellent Youth Foundation of Guangdong Scientific Committee (2021B1515020037), the Program of the Department of Natural Resources of Guangdong Province, China (GDNRC [2021]53 and GDNRC [2021]49), Natural Science Foundation of Guangdong Province (2019A1515011670) the 111 Project (B17018) and Belarusian Republican Foundation for Fundamental Research (grant X22KI-11). This project was also financially supported by the Theme-Based Research Scheme (Project No. T21-604/19-R) of the Research Grants Council (RGC) of the Hong Kong Special Administrative Region, China.

We are thankful to Dr. Riming Huang and Dr. Xiaodan Shi for their help in structural analysis. And we also thank to Xiong Li, Xiaoyong Chen, Weixuan Huang, Yufeng Gong and Qiuhong Kong for guidance on the experimental scheme and Sanshu Biotechnology for its analysis of monosaccharide composition and methylation data.

Appendix A. Supplementary data

Supplementary data to this article can be found online at https://doi.org/10.1016/j.foodres.2022.111267.

References

Auh, J. H., & Madhavan, J. (2021). Protective effect of a mixture of marigold and rosemary extracts on UV-induced photoaging in mice. *Biomedicine Pharmacotherapy, 135*, Article 111178. https://doi.org/10.1016/j.biopha.2020.111178

Benbow, U., & Brinckerhoff, C. E. (1997). The AP-1 site and MMP gene regulation: What is all the fuss about? *Matrix Biology, 15*(8–9), 519–526. https://doi.org/10.1016/s0945-053x(97)90026-3

Cao, C. W., Xiao, Z. C., Wu, Y. L., & Ge, C. R. (2020). Diet and skin aging-from the perspective of food nutrition. *Nutrients, 12*(3), 870. https://doi.org/10.3390/nu12030870

Chang, X., Shen, C. Y., & Jiang, J. G. (2021). Structural characterization of novel arabinoxylan and galactoarabinan from citron with potential antitumor and immunostimulatory activities. *Carbohydrate Polymers, 269*. https://doi.org/10.1016/j.carbpol.2021.118331

Chen, X. Y., Li, X., Sun, W. D. X., Zhu, B. Y., You, L. J., & Hileuskaya, K. (2021a). Polysaccharides from *Sargassum fusiforme* after UV/H_2O_2 degradation effectively ameliorate dextran sulfate sodium-induced colitis. *Food & Function, 12*(23), 11747–11759. https://doi.org/10.1039/d1fo02708e

Chen, X. Y., You, L. J., Ma, Y. X., Zhao, Z. G., & Kulikouskaya, V. (2021b). Influence of UV/H_2O_2 treatment on polysaccharides from *Sargassum fusiforme*: Physicochemical properties and RAW 264.7 cells responses. *Food Chemical. Toxicology, 153*, Article 112246. https://doi.org/10.1016/j.fct.2021.112246

Chen, X. Y., Zhang, R. F., Li, Y. Z., Li, X., You, L. J., Kulikouskaya, V., & Hileuskaya, K. (2020). Degradation of polysaccharides from *Sargassum fusiforme* using UV/H_2O_2 and its effects on structural characteristics. *Carbohydrate Polymers, 230*. https://doi.org/10.1016/j.carbpol.2019.115647

Cheng, Y., Xie, Y., Ge, J. C., Wang, L., Peng, D. Y., Yu, N. J., … Chen, W. D. (2021). Structural characterization and hepatoprotective activity of a galactoglucan from *Poria cocos*. *Carbohydrate Polymers, 263*, Article 117979. https://doi.org/10.1016/j.carbpol.2021.117979

Cong, Q. F., Xiao, F., Liao, W. F., Dong, Q., & Ding, K. (2014). Structure and biological activities of an alginate from *Sargassum fusiforme*, and its sulfated derivative. *International Journal of Biological Macromolecules, 69*, 252–259. https://doi.org/10.1016/j.ijbiomac.2014.05.056

Crispin, I. G., Hernandez, R. L., Ramirez, S. C., Sandoval, C. O., Lobato, C. C., & Vernon, C. E. J. (2019). Influence of purification on physicochemical and emulsifying properties of tamarind (*Tamarindus indica L.*) seed gum. *Food Hydrocolloids, 93*, 402–412. https://doi.org/10.1016/j.foodhyd.2019.02.046

Cui, S. W. (2005). *Structural Analysis of Polysaccharides*. Structural Analysis of Polysaccharides (Chapter 3).

DeRamos, C. M., Irwin, A. E., Nauss, J. L., & Stout, B. E. (1997). ^{13}C NMR and molecular modeling studies of alginic acid binding with alkaline earth and lanthanide metal ions. *Inorganica Chimica Acta, 256*(1), 69–75. https://doi.org/10.1016/S0020-1693(96)05418-7

Duan, X., Wu, T., Liu, T., Yang, H., Ding, X. J., Chen, Y., & Mu, Y. Z. (2019). Vicenin-2 ameliorates oxidative damage and photoaging via modulation of MAPKs and MMPs signaling in UVB radiation exposed human skin cells. *Journal of Photochemistry & Photobiology B Biology, 190*, 76–85. https://doi.org/10.1016/j.jphotobiol.2018.11.018

Dubois, M., Gilles, K. A., Hamilton, J. K., Rebers, P. A., & Smith, F. (1956). Colorimetric method for determination of sugars and related substances. *Analytical Chemistry, 28*(3), 350–356. https://doi.org/10.1021/ac60111a017

Filip, A., Daicoviciu, D., Clichici, S., Bolfa, P., Catoi, C., Baldea, I., … Postescu, I. D. (2011). The effects of grape seeds polyphenols on SKH-1 mice skin irradiated with multiple doses of UV-B. *Journal of Photochemistry and Photobiology B: Biology, 105*(2), 133–142. https://doi.org/10.1016/j.jphotobiol.2011.08.002

Hao, H. L., Han, Y., Yang, L. H., Hu, L. M., Duan, X. Y., Yang, X., & Huang, R. M. (2019). Structural characterization and immunostimulatory activity of a novel polysaccharide from green alga *Caulerpa racemosa* var *peltata*. *International Journal of Biological Macromolecules, 134*, 891–900. https://doi.org/10.1016/j.ijbiomac.2019.05.084

Helfrich, Y. R., Sachs, D. L., & Voorhees, J. J. (2008). Overview of skin aging and photoaging. *Dermatology nursing, 20* (3), 177-183; quiz 184. https://www.researchgate.net/publication/51423323.

Holtan, S., Bruheim, P., & Skjak, B. G. (2006). Mode of action and subsite studies of the guluronan block-forming mannuronan C-5 epimerases AlgE1 and AlgE6. *The Biochemical Journal, 395*(2), 319–329. https://doi.org/10.1042/BJ20051804

Ji, D. S., You, L. J., Ren, Y. L., Wen, L. R., Zheng, G. Q., & Li, C. (2017). Protective effect of polysaccharides from *Sargassum fusiforme* against UVB-induced oxidative stress in HaCaT human keratinocytes. *Journal of Functional Foods, 36*, 332–340. https://doi.org/10.1016/j.jff.2017.06.051

Kong, Q. H., Zhang, R. F., You, L. J., Ma, Y. X., Liao, L., & Pedisi, S. (2021). *In vitro* fermentation characteristics of polysaccharide from *Sargassum fusiforme* and its modulation effects on gut microbiota. *Food and Chemical Toxicology, 151*, Article 112145. https://doi.org/10.1016/j.fct.2021.112145

Kwon, K. R., Alam, M. B., Park, J. H., Kim, T. H., & Lee, S. H. (2019). Attenuation of UVB-induced photo-aging by polyphenolic-rich spatholobus suberectus stem extract via modulation of MAPK/AP-1/MMPs signaling in human keratinocytes. *Nutrients, 11*(6), 1341. https://doi.org/10.3390/nu11061341

Lee, K., Kim, H. J., Kim, S. A., Park, S. D., Shim, J. J., & Lee, J. L. (2021). Exopolysaccharide from *Lactobacillus plantarum* HY7714 protects against skin aging through skin-gut axis communication. *Molecules, 26*(6), 1651. https://doi.org/10.3390/molecules26061651.

Li, F., Feng, K. L., Yang, J. C., He, Y. S., & Wu, D. T. (2020). Polysaccharides from dandelion (*Taraxacum mongolicum*) leaves: Insights into innovative drying techniques on their structural characteristics and biological activities. *International Journal of Biological Macromolecules, 167*, 995–1005. https://doi.org/10.1016/j.ijbiomac.2020.11.054

Li, Y., Yang, F., Gao, P., Jiang, Q., Xu, Y., Wu, F., & Xia, W. (2018). Purification and structure identification of algin in *Sargassum fusiform*. *Food science and technology, 43*(05), 219–223. https://doi.org/10.13684/j.cnki.spkj.2018.05.039.

Li, Z. R., Jia, R. B., Wu, J., Lin, L. Z., Ou, Z. R., Liao, B. W., … Zhao, M. M. (2021). *Sargassum fusiforme* polysaccharide partly replaces acarbose against type 2 diabetes in rats. *International Journal of Biological Macromolecules, 170*, 447–458. https://doi.org/10.1016/j.ijbiomac.2020.12.126

Lindsay, H. (1973). A colorimetric estimation of reducing sugars in potatoes with 3,5-dinitrosalicylic acid. *Potato Research, 16*(3), 176–179. https://doi.org/10.1007/BF02356048

Liu, L. L. (2014). Modification of reduction method about uronic acids in acidic polysaccharides. *Chinese Journal of Marine Drugs, 33*(04), 1–7. https://doi.org/10.13400/j.cnki.cjmd.2014.04.001.

Liu, Y., Ye, Y. F., Hu, X. B., & Wang, J. H. (2021). Structural characterization and anti-inflammatory activity of a polysaccharide from the *lignified okra*. *Carbohydrate Polymers, 265*, Article 118081. https://doi.org/10.1016/j.carbpol.2021.118081

Masaki, H., Izutsu, Y., Yahagi, S., & Okano, Y. (2009). Reactive oxygen species in HaCaT keratinocytes after UVB irradiation are triggered by intracellular Ca(2+) levels. *Journal of Investigative Dermatology Symposium Proceedings, 14*(1), 50–52. https://doi.org/10.1038/jidsymp.2009.12

Michalak, M., Pierzak, M., Krecisz, B., & Suliga, E. (2021). Bioactive compounds for skin health: A review. *Nutrients, 13*(1). https://doi.org/10.3390/nu13010203

Misawa, E., Tanaka, M., Saito, M., Nabeshima, K., Yao, R., Yamauchi, K., … Furukawa, F. (2017). Protective effects of Aloe sterols against UVB-induced photoaging in hairless mice. *Photodermatol Photoimmunol Photomed, 33*(2), 101–111. https://doi.org/10.1111/phpp.12286

Nelly, B., & Gustav, A. H. (1973). New method for quantitative determination of uronic acids. *Analytical Biochemistry, 54*(2), 484–489. https://doi.org/10.1016/0003-2697(73)90377-1

Nie, J. G., Chen, D. T., Lu, Y. B., & Dai, Z. Y. (2021). Effects of various blanching methods on fucoxanthin degradation kinetics, antioxidant activity, pigment composition, and sensory quality of *Sargassum fusiforme*. *Lwt, 143*. https://doi.org/10.1016/j.lwt.2021.111179

Penna, I., Albanesi, E., Bertorelli, R., Bandiera, T., & Russo, D. (2019). Cytoprotective, anti-inflammatory, and antioxidant properties of high-molecular-weight hyaluronan enriched with red orange extract in human fibroblasts exposed to ultra violet light B irradiation. *Biotechnology and Applied Biochemistry, 66*(3), 273–280. https://doi.org/10.1002/bab.1722

Rigel, D. S. (2008). Cutaneous ultraviolet exposure and its relationship to the development of skin cancer. *Journal of the American Academy of Dermatology, 58*(5 Suppl 2), S129–S132. https://doi.org/10.1016/j.jaad.2007.04.034

Sanjeewa, K. K. A., Lee, J. S., Kim, W. S., & Jeon, Y. J. (2017). The potential of brown-algae polysaccharides for the development of anticancer agents: An update on anticancer effects reported for fucoidan and laminaran. *Carbohydrate Polymers, 177*, 451–459. https://doi.org/10.1016/j.carbpol.2017.09.005

Shao, P., Feng, J. R., Sun, P. L., Xiang, N., Lu, B. Y., & Qiu, D. (2020). Recent advances in improving stability of food emulsion by plant polysaccharides. *Food Research International, 137*, Article 109376. https://doi.org/10.1016/j.foodres.2020.109376

Shi, Q., Yan, J. Y., Jiang, B., Chi, X. J., Wang, J. H., Liang, X. M., & Ai, X. J. (2021). A general strategy for the structural determination of carbohydrates by multi-dimensional NMR spectroscopies. *Carbohydrate Polymers, 267*, Article 118218. https://doi.org/10.1016/j.carbpol.2021.118218

Son, J., & Lee, S. Y. (2020). Ursonic acid exerts inhibitory effects on matrix metalloproteinases via ERK signaling pathway. *Chemico-Biological Interactions, 315*, Article 108910. https://doi.org/10.1016/j.cbi.2019.108910

Sun, F. F., Niu, H., Wang, D. D., Wu, Y. Y., Mu, H. B., Ma, L. L., & Duan, J. Y. (2017). Novel moisture-preserving derivatives of hyaluronan resistant to hyaluronidase and protective to UV light. *Carbohydrate Polymers, 157*, 1198–1204. https://doi.org/10.1016/j.carbpol.2016.10.086

Verma, A., Kushwaha, H. N., Srivastava, A. K., Srivastava, S., Jamal, N., Srivastava, K., & Ray, R. S. (2017). Piperine attenuates UV-R induced cell damage in human keratinocytes via NF-κB, Bax/Bcl-2 pathway: An application for photoprotection. *Journal of Photochemistry and Photobiology B: Biology, 172*, 139–148. https://doi.org/10.1016/j.jphotobiol.2017.05.018

Wang, L., Oh, J. Y., Kim, Y. S., Lee, H. G., Lee, J. S., & Jeon, Y. J. (2020). Anti-photoaging and anti-melanogenesis effects of fucoidan isolated from *Hizikia fusiforme* and its underlying mechanisms. *Marine Drugs, 18*(8), 427. https://doi.org/10.3390/md18080427

Wang, L., Zhang, B., Xiao, J., Huang, Q., Li, C., & Fu, X. (2018). Physicochemical, functional, and biological properties of water-soluble polysaccharides from Rosa roxburghii Tratt fruit. *Food Chemistry, 249*, 127–135. https://doi.org/10.1016/j.foodchem.2018.01.011

Wang, N. F., Jia, G. G., Wang, X. F., Liu, Y., & Xiao, D. G. (2020). Fractionation, structural characteristics and immunomodulatory activity of polysaccharide fractions from asparagus (*Asparagus officinalis L.*) skin. *Carbohydrate Polymers, 256*(2), Article 117514. https://doi.org/10.1016/j.carbpol.2020.117514

Wen, L. R., Gao, Q., Ma, C. W., Ge, Y. Z., You, L. J., Liu, R. H., … Liu, D. (2016). Effect of polysaccharides from *Tremella fuciformis* on UV-induced photoaging. *Journal of Functional Foods, 20*, 400–410. https://doi.org/10.1016/j.jff.2015.11.014

Wen, L. R., Shi, D. D., Zhou, T., Tu, J. M., He, M. Y., Jiang, Y. M., & Yang, B. (2020). Identification of two novel prenylated flavonoids in mulberry leaf and their bioactivities. *Food Chemistry, 315*, Article 126236. https://doi.org/10.1016/j.foodchem.2020.126236

Xiao, Z. B., Yang, S. T., Chen, J. L., Li, C. Y., Zhou, C. X., Hong, P. Z., … Qian, Z. J. (2020). Trehalose against UVB-induced skin photoaging by suppressing MMP expression and enhancing procollagen I synthesis in HaCaT cells. *Journal of Functional Foods, 74*. https://doi.org/10.1016/j.jff.2020.104198

Xie, F., Zhang, H., Nie, C., Zhao, T. L., & Ai, L. Z. (2021). Structural characteristics of tamarind seed polysaccharides treated by high-pressure homogenization and their effects on physicochemical properties of corn starch. *Carbohydrate Polymers, 262*, Article 117661. https://doi.org/10.1016/j.carbpol.2021.117661

Ye, Y. H., Ji, D. S., You, L. J., Zhou, L., Zhao, Z. G., & Brennan, C. (2018). Structural properties and protective effect of *Sargassum fusiforme* polysaccharides against ultraviolet B radiation in hairless Kun Ming mice. *Journal of Functional Foods, 43*, 8–16. https://doi.org/10.1016/j.jff.2018.01.025

Youn, L. J., Kyung, K. O., Jeongmin, L., Jae, L. M., Namgil, K., & Kwan, H. J. (2014). Protective effect of the standardized green tea seed extract on UVB-induced skin photoaging in hairless mice. *Nutrition Research & Practice, 8*(4), 398–403. https://doi.org/10.4162/nrp.2014.8.4.398

Youssouf, L., Lallemand, L., Giraud, P., Soulé, F., Archana, B. L., Meilhac, O., … Couprie, J. (2017). Ultrasound-assisted extraction and structural characterization by NMR of alginates and carrageenans from seaweeds. *Carbohydrate Polymers, 166*, 55–63. https://doi.org/10.1016/j.carbpol.2017.01.041

Zhang, H., Wang, J. Q., Nie, S. P., Wang, Y. X., Cui, S. W., & Xie, M. Y. (2015). Sulfated modification, characterization and property of a water-insoluble polysaccharide from Ganoderma atrum. *International Journal of Biological Macromolecules, 79*, 248–255. https://doi.org/10.1016/j.ijbiomac.2015.04.070

Zhang, R., Zhang, X. X., Tang, Y. X., & Mao, J. L. (2020). Composition, isolation, purification and biological activities of *Sargassum fusiforme* polysaccharides: A review. *Carbohydrate Polymers, 228*, Article 115381. https://doi.org/10.1016/j.carbpol.2019.115381

Zhang, X., Huo, D., Cao, C. L., Li, Y. T., Liang, Y., Li, B., & Li, L. (2019). Preliminary characterization, antioxidant and α-glucosidase inhibitory activities of polysaccharides from *Mallotus furetianus*. *Carbohydrate Polymers, 215*, 307–315. https://doi.org/10.1016/j.ijbiomac.2015.04.070

Zhi, Q., Lei, L., Li, F. H., Zhao, J. C., Yin, R., & Ming, J. (2020). The anthocyanin extracts from purple-fleshed sweet potato exhibited anti-photoaging effects on ultraviolent B-irradiated BALB/c-nu mouse skin. *Journal of Functional Foods, 64*, Article 103640. https://doi.org/10.1016/j.jff.2019.103640